Journal of Alloys and Compounds 509 (2011) 440–446

Contents lists available at ScienceDirect

Journal of Alloys and Compounds

journal homepage: www.elsevier.com/locate/jallcom

Effect of carbon doping on microstructure, electronic and magnetic properties of Cr:AlN films

F. Zeng[a,*], C. Chen[a], B. Fan[a], Y.C. Yang[a], P.Y. Yang[a], J.T. Luo[a], F. Pan[a], W.S. Yan[b]

[a] Key Laboratory of Advanced Materials (MOE), Department of Materials Science and Engineering, Tsinghua University, Beijing 100084, People's Republic of China
[b] National Synchrotron Radiation Laboratory (NSRL), University of Science & Technology of China, Hefei 230029, People's Republic of China

ARTICLE INFO

Article history:
Received 13 June 2010
Received in revised form 8 September 2010
Accepted 9 September 2010
Available online 22 September 2010

Keywords:
Magnetic films and multilayers
NEXAFS
Magnetic measurements
Electronic transport
Semiconductors

ABSTRACT

Carbon was doped into Cr:AlN films. Microstructure analysis demonstrated that the Cr atom kept at AlN lattice when carbon content was lower. The doped carbon atoms formed graphite phases and C–N clusters dispersing in the films, which influenced the electric and magnetic properties significantly. When the resistivity was around 10^5–10^7 Ω cm under an alternating current (AC) frequency of 210 Hz, it increased with increasing carbon content, and when the resistivity was around 10^3 Ω cm under a higher AC frequency of 800 kHz, it decreased with increasing carbon content. The magnetisms for the carbon-doped samples are stronger than those of samples without carbon doping. The atomic magnetic moment (AMM) of the sample with a carbon content of 2.3 at.% was the highest ($0.4\mu_B$/Cr). It was proposed that atomic migration of carbon might have occurred under high AC frequency. The formation of C–N compounds could consume part of the available nitrogen and then increased the density of N vacancy in the Cr:AlN lattice, which is favorable for coupling among bound magnetic polarons (BMP).

1. Introduction

Dilute doping into wide band-gap semiconductors has been intensively investigated in the past 15 years because it produces numerous novel properties and possible applications, such as materials used in spintronics and nonvolatile storage [1–3]. These novel properties are significantly and extensively sensitive to various defects. Doping can induce defects like atom substitution, interstitial atom, vacancy, cluster and deformation. It should be careful when distinguishing the defects states, their formation mechanisms and effect on the properties. It is necessary to combine many characteristic methods for detailed analysis and determination. Furthermore, scientists are attempting new doping new materials to introduce various defects, produce new phenomena and enhance properties. Normally, in oxides and nitride compounds used in spintronics, the local magnetic ordering relates to the 3d and 4f transition metals, which bring local moments into the solid. These local moments couple with each other to realize macroscopic magnetism. However, nonmagnetic materials including carbon are currently used to generate spin polarization [4].

Carbon is a typical polymorphic material. Graphene and carbon nanotubes have been intensively and extensively studied and carbon doping into a semiconductor has attracted much attention recently. Yuan et al. obtained a two-dimensional hole gas in carbon-doped (1 0 0) GaAs/$Al_{0.4}Ga_{0.6}As$ square quantum well and they were able to enhance effective *g*-factor as well [5]. Lim et al. fabricated nano-carbon doped MgB_2 bulks materials and improved the critical current density (J_c) under a high magnetic field [6]. Kwak et al. predicted that the carbon dopants can become magnetic under confinement in ZnO nanocrystals and nanowires [7]. Herng et al. obtained p-type magnetic ZnO using ion implantation [8]. Due to the polymorphism of carbon in these semiconductors, the modulation mechanisms of these properties, including carriers, local moment, and transport behaviors under magnetic field, vary significantly. Based on this, it is deserved to study extensively the effects of carbon on more semiconductors.

Wurtzite AlN is a wide-gap semiconductor with a high melting point and high thermal conductivity, which are advantages for high power devices. Cr-doped AlN has been found having high magnetic Curie temperature which is favorable for spintronics [9] and high piezoelectric response which is favorable for surface acoustic waves devices [10]. In this paper, we attempted to introduce carbon dopant into Cr:AlN and study its effect on electric and magnetic properties. After carbon doping, it was found that the conductivity varied greatly under different alternating current (AC) frequencies and that the magnetism was enhanced obviously.

2. Experimental details

The carbon and chromium co-doped AlN films were prepared using DC reactive sputtering method. The target was aluminum plate on which small graphite and

* Corresponding author. Fax: +86 10 62771160.
E-mail address: zengfei@mail.tsinghua.edu.cn (F. Zeng).

0925-8388/$ – see front matter © 2010 Elsevier B.V. All rights reserved.
doi:10.1016/j.jallcom.2010.09.052

chromium strips were placed. The compositions of C and Cr were modulated by modifying the amount of the strips. The base pressure was 4×10^{-5} Pa. The substrate was Si(1 1 1) and the substrate temperature was 250 °C. During the deposition process, the partial pressure of nitrogen and argon were kept at 0.3 and 0.5 Pa, respectively. The deposition rate was about 5 nm/min. The total thickness was kept at about 200 nm.

The contents of Cr and C were determined using inductively coupled plasma-atomic emission spectroscopy (ICP-AES) using Shimadzu ICPS-7510. The content of Cr was monitored to be about 7.4 at.%, and that of C was 0, 2.3, 3.2 and 4.7 at.%. The structures were characterized by X-ray diffraction (XRD), Raman spectroscopy, and Cr, N and C *K*-edge X-ray absorption near edge structure (XANES). The large-angle and low-angle XRD measurements were performed on Rigaku D/max-rB equipment. Raman scattering experiments were performed at room temperature in backscattering and close-to-90° configuration using Micro-Raman spectroscopy (RM 2000, Reinishaw). An Ar^+ laser of 514.5 nm was used as an excitation source. The resolution of the Raman shift is 1 cm^{-1}. The XANES spectra were measured in the fluorescence mode using synchrotron radiation at the beam-line U7C of National Synchrotron Radiation Facility (NSRF). The magnetic property was characterized at room temperature using a vibrating sample magnetometer (VSM) with a resolution of 10^{-7} emu, which is integrated in the physical property–measurement system (PPMS) of Quantum Design cooperation. The monolayer samples, as well as Al–AlN–Al capacitor structures, with a top electrode consisting of a 0.3 mm Al disk, were also prepared to measure the resistivity at an AC frequency range of 200 Hz to 1 MHz.

3. Results and discussions

3.1. Microstructures

The Cr:AlN films without carbon had a wurtzite structure with an apparent (0 0 2) texture (Fig. 1). Such structure was maintained after a small amount (up to 3.2 at.%) of carbon was doped. The value of lattice constant *c*, which was calculated from the XRD spectra, is 4.99 Å for the sample without carbon, and it was 5.01 Å and 5.06 Å for the samples with 2.3 and 3.2 at.% of carbon, respectively. The intensity of the (0 0 2) peak dropped dramatically for the two later samples. For the sample with 4.7 at.% of carbon, the diffraction pattern of AlN was unclear. These features indicated that the specimen doped with carbon content lower than 3.2 at.% induced tensile stress perpendicular to the film plane and then elongated the lattice constant *c*. The direction perpendicular to the film plan is practically unconstrained, which might be one reason for the strain observed along the *c* direction. There was no arching or cracking occurred, which might be due to the limited thickness of 200 nm and good adhesion on the substrate with high temperature.

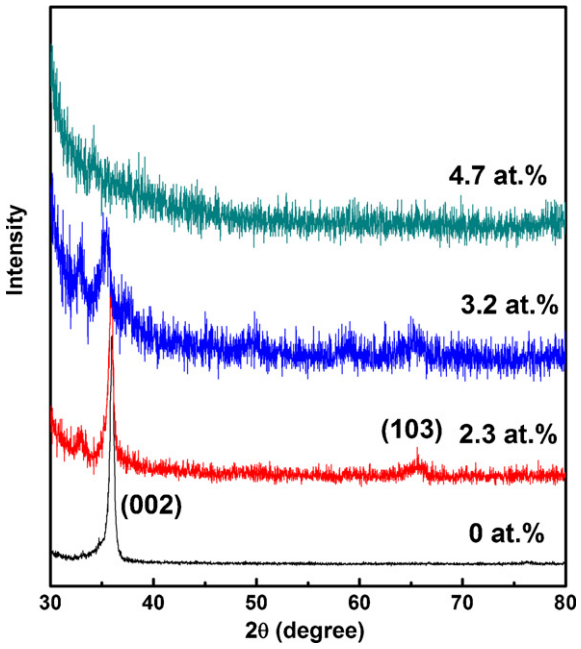

Fig. 1. XRD spectra of Cr-doped AlN films with the carbon content labeled beside every curve.

The neighboring atomic environments were important and were studied using XANES spectra (Figs. 2–4). Since the samples were still wurtzite structures when the carbon content was lower than 3.2 at.%, the atomic environments around the Cr atom was first considered in order to examine if the positions of the Cr atoms were modulated by carbon doping. The Cr *K*-edge XANES spectra and some instances which are simulated using FEFF8 code [11,12] are presented in Fig. 2. Characteristic peaks were labeled as A, B, C and D.

The features of Fig. 2(a1) for the sample without carbon are consistent with our previous study [13,14]. As discussed in Refs. [13,14], peak A in Fig. 2(a1) was due to the transition from Cr 1s electron to Al 3d–O 4p hybridized states occurring in low

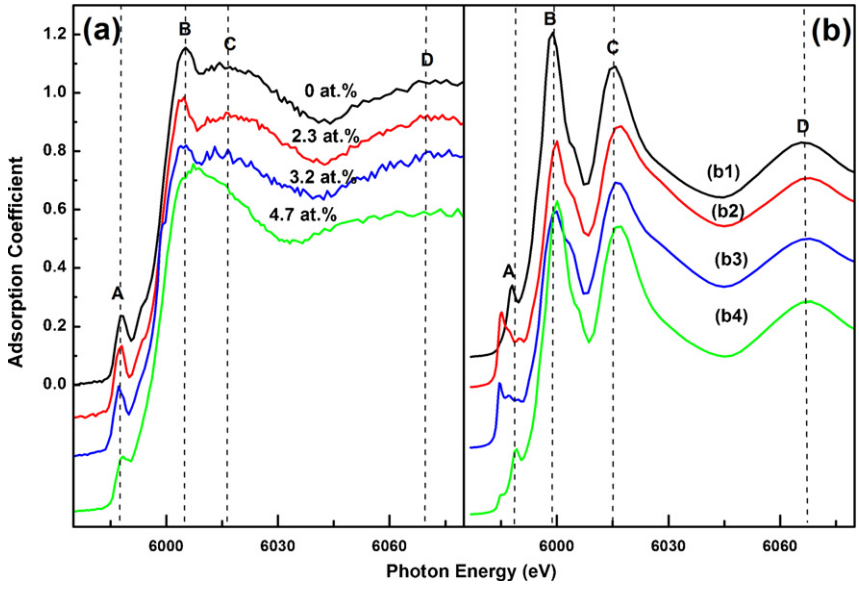

Fig. 2. Variation of the Cr *K*-edge XANES. (a) Experimental results for various carbon content; (b) simulated spectra using FEFF8 code (b1) no carbon doped; (b2) substitution of an Al atom in the second nearest neighbor by a Cr atom; (b3) substitution of an N atom in the first nearest neighbor by a carbon atom; (b4) substitution of an Al atom in the second nearest neighbor by a C atom.

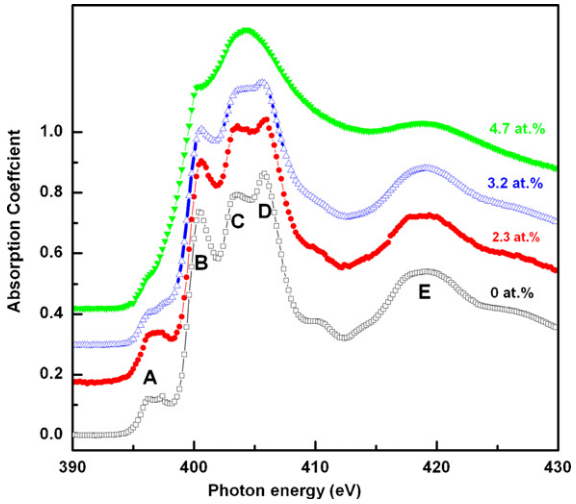

Fig. 3. Variation of the N *K*-edge XANES with the carbon content labeled beside every curve.

symmetry ligand fields such as the tetrahedral ligand field [15,16]. In the N *K*-edge XANES spectra (Fig. 3), besides the characteristic peaks of wurtzite structure above the photon energy of 400 eV, a low intensity peak appears at 397 eV (peak A in Fig. 3) which was not presented in pure AlN sample [17]. It corresponded to the split e_g and t_{2g} spin-up and spin-down states of Cr hybridized with N 2p states. Characteristic peaks A in both the Cr *K*-edge XANES spectra and the N *K*-edge XANES spectra demonstrated that the Cr atom was in the center of a tetrahedron while the N atoms were at the corners. The site of N might be vacancy or substituted by C atom. Since Fig. 2(a2) and (a3) had similar features with that of Fig. 2(a1), the Cr atoms were regarded principally to have dissolved into the AlN matrix and substituted the Al atoms. However, the formation of Cr carbide could not be excluded because Fig. 2(a2) also resembled some spectra of the Cr carbides [18–20].

Consequently, the C *K*-edge XANES spectra (Fig. 4) and the Raman spectra (Fig. 5) were examined to confirm this hypothesis. Comparing the results in Fig. 4 with many carbon-transition metal films [21], no apparent features of carbide species were found. There were two characteristic peaks in the region with Raman shift lower than 1000 cm^{-1} (Fig. 5). The first was at around 200 cm^{-1} and the second was at around 580–590 cm^{-1}. The two Raman

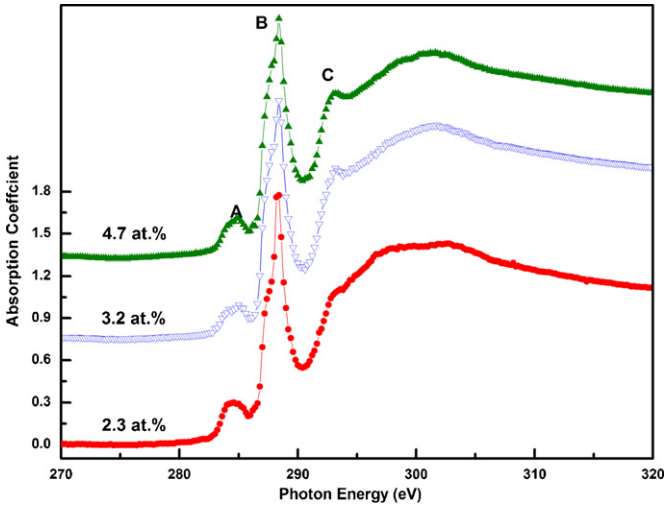

Fig. 4. Variation of C *K*-edge XANES with the carbon content labeled beside every curve.

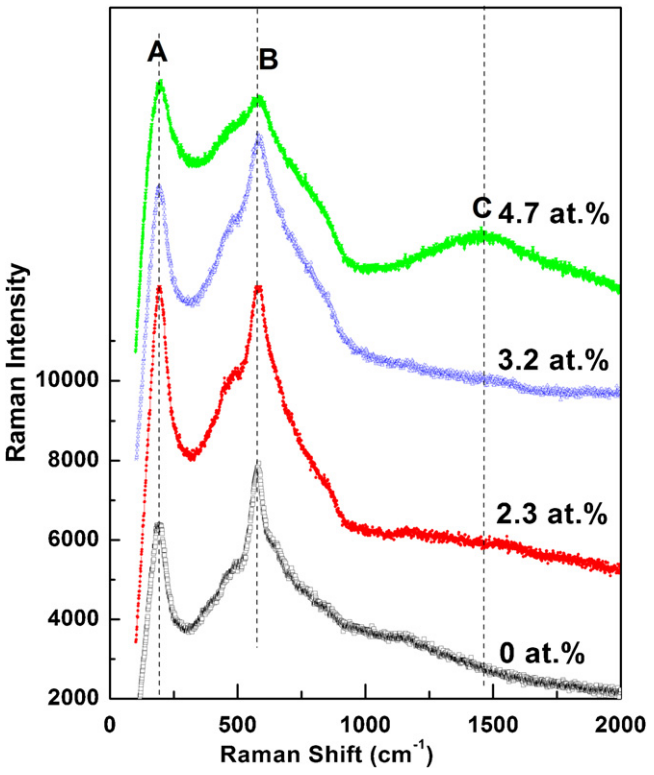

Fig. 5. Variation of Raman shift (cm^{-1}) with the carbon content labeled beside every curve.

peaks were much lower than those of pure AlN (about 248.6 and 657.4 cm^{-1}). They corresponded to E_2(low) and E_2(high) models, which were excited by the electric field perpendicular to the *c* axis [22]. These two values are consistent with the results of Kaindl et al. [23] which were due to Cr doping. This further demonstrated that the Cr atoms located in the AlN crystal lattice. Additionally, the stress and deficiency of N or Cr could move the Raman shifts [23–25]. Chen et al. have demonstrated that a tensile stress would induce Raman spectra blue-shifted for *c*-axis texture films [23]. Bernard et al. have showed that N vacancy is another factor for increase of Raman shift [25]. In Table 1, peaks A and B in Fig. 5 move a little toward higher values when carbon was doped. The movements were small and apparent features of Cr carbide were not observed in Fig. 4 so that the consumption of Cr atoms by the doped carbon was not considered. These small movements should come from tensile stress along *c*-axis, which was also reflected by the increase of lattice constant *c* (Fig. 1), or N vacancy in the films doped by carbon.

Although the environment of the Cr atom was principally determined from previous discussion, it should have been modified to

Table 1
Comparison of peaks A, B and C in Raman spectroscopy (Fig. 5).

	Content of carbon			
	0	2.3 at.%	3.2 at.%	4.7 at.%
Peak A				
Intensity	6376	10987	8682	9170
Raman shift (cm^{-1})	199.43	192.69	205.2	200.4
Peak B				
Intensity	7834	11111	10145	8763
Raman shift (cm^{-1})	578.45	580.38	592.88	589
Peak C				
Intensity				5360
Raman shift (cm^{-1})				1470

Table 2
Comparison of peak A and peak B in the Cr *K*-edge XANES (Fig. 2(a)).

	Content of carbon			
	0	2.3 at.%	3.2 at.%	4.7 at.%
Peak A				
Intensity	0.236819	0.278747	0.28679	0.19028
Photon energy (eV)	5987.68	5988.03	5987.14	5988.36
Peak B				
Intensity	1.1517	1.13102	1.11029	1.19206
Photon energy (eV)	6005.21	6004.79	6005.33	6007.22

some extent by the doped carbon. Variations of the characteristic peaks in Fig. 2(a) are listed in Table 2. Modification for the Cr environment could be observed in three ways. The first was the substitution of neighboring atom around Cr atom by another atom. Simulations in Fig. 2(b) considered several substitutions. Fig. 2(b1) was a typical simulation of the Cr *K*-edge XANES pattern of Cr:AlN without considering any defects, such as substitution and vacancy. It was consistent with the main features of Fig. 2(a1). The experimental and simulated spectra were also consisted with the features of Cr-XANES spectra in other studies on the Cr-doped AlN and GaN [26,27]. Unlike studies by Hashimoto et al. [27], in our experiment, it did not find formation of CrN though the Cr content was high because the pre-edge A and main peak B, which correspond to the Cr 1s core state to the 3d-like state and 4p-like state [27], were clearly. A step (around 5994 eV, as shown in Fig. 2(a)), which corresponds to the transitions from Cr 1s state to anti-bonding state originated from hybridizing between Cr 4s state and N 2s state with the partial mixing of N 2p state [27], was also discernable. Combining results of ours and Refs. [26,27], we determined that no evident CrN was formed at least for the samples with C content lower than 4.7 at.%. Fig. 2(b2) showed the simulation of substituting an Al atom by a Cr atom in the second nearest neighbor of the Cr absorption center. Peak A moved to a lower photon energy and the intensity of peak C increased. These features were more different from Fig. 2(a1). This also occurred in the simulation shown in Fig. 2(b3), where an N atom was substituted by a C atom in the first nearest neighbor of the Cr absorption center. These two results (Fig. 2(b2) and (b3)) indicate that the tetrahedrons with Cr in the center were isolated from each other and that it was unlikely for the carbon to substitute the N atom at the corner of the Cr–N tetrahedrons. Thus, the Cr–C bond was unlikely to appear in the first neighbor of the Cr atoms. Furthermore, substitution of an Al atom by a C atom in the second nearest neighbor of the Cr absorption center was simulated in Fig. 2(b4). The positions and relative intensity of peaks A, B, C, D were similar to Fig. 2(a1) and (b1). This indicated that the carbon atom could appear in the Al position near the Cr–N tetrahedron or at some position relative far from the Cr atom. Besides, Cr or C atoms in the interstitial positions were also simulated. The results found that the features of pre-edge and the main peaks were much different from the experimental results.

The second way was the deformation of the Cr–N tetrahedron. In Table 2, the relative intensity between peak A and B in Fig. 2(a) were compared. The intensity of peak A increased slightly until the carbon content reaches to 4.7 at.%. Based on the discussion of the XRD spectra, a tensile stress was apparently induced when the carbon was lower than 3.2 at.%. Stress could also deform the N tetrahedron surrounding the Cr atom, lowering the symmetry of the ligand field. Consequently, it enhanced the probability of the 1s to 3d transition, and then the intensity of peak A in Fig. 2(a2) and (a3). However, this deformation could not be infinite. When the carbon content increased to 4.7 at.%, the disorder was so intensive that the absorption resonance was weakened very much (Fig. 2(a4)).

The third way was the introduction of more N vacancies. In our experiments, the substrate temperature was 250 °C which was not sufficient to form a good C–N crystal. Since the sputtering process was far from equilibrium, many C–N bonds with sp^1, sp^2, or sp^3 hybrids could be formed. The doped carbon consumed part of nitrogen to form C–N compounds, and then leave more N vacancies in the AlN lattice.Apart from the influence on the atomic environment of the Cr atom, the state of carbon was another important point should be understood in depth. Fig. 4 shows the C *K*-edge XANES spectra with various carbon contents. Three characteristic peaks were found around 284.5 eV (peak A), 288.4 eV (peak B) and 293.2 eV (peak C). Their relative intensities and positions are listed in Table 3. Peaks A and C in Fig. 4 should correspond to the π^* and σ^* exciton peaks, respectively [21,28–30]. They were caused by the $1s \rightarrow 2p$ electron transitions, including $1s \rightarrow \pi^*$ and $1s \rightarrow \sigma^*$ transitions which normally appear in the graphite phase [31]. The peaks between peaks A and C should be due to the carbon–nitrogen compounds [21,28]. These results indicate that the samples used in this study contained a graphite phase. When the doping content of carbon was low, the fraction of the graphite phase was very low. For example, for the sample with a carbon content of 2.3 at.%, peak C was weak (in Fig. 4) and the contribution of the graphite phase to the Raman shift was not discernible (Fig. 5). When the carbon content increased to 4.7 at.%, the peak C increased (Fig. 4), and a broad Raman peak around 1470 cm^{-1}, which is due to the resonant model of the carbon ring in the graphite [32,33], was observed (Fig. 5).

Aside from the graphite phase of the samples, the carbon atoms had other states. Several works have discussed this issue [21,28,34]. The main feature of ours is that peak B rose more sharply and had much higher intensity than peaks A and C (Fig. 5). The ratios of peak B to peak A were 6.05, 3.21 and 2.31 for the samples doped by carbon. The ratios of peak B to peak C were 1.64, 1.30 and 1.27. There was a shoulder around the 286 eV slightly lower than peak B. These features were much different from the carbidic species and the modified environment of carbon by the mixed transition metals [21]. The features of peak B were consistent with the results of Moreau et al. in both experimental and theoretical modulation [28]. Therefore, the C–N compounds, which were mainly composed of C_3N_4 [28], were formed during the deposition process.

In Fig. 6, N and C *K*-edge XANES spectra were further simulated using FEFF8 code. Fig. 6(a) shows N *K*-edge XANES spectra, including AlN and Cr:AlN. For Cr:AlN, one Cr atom substituted one Al atom

Table 3
Comparison of peaks A, B and C in the C *K*-edge XANES (Fig. 4).

	Content of carbon		
	2.3 at.%	3.2 at.%	4.7 at.%
Peak A			
Intensity	0.293	0.612	1.059
Photon energy (eV)	284.4	285	284.8
Peak B			
Intensity	1.773	1.966	2.45
Photon energy (eV)	288.4	288.4	288.4
Peak C			
Intensity	1.081	1.514	1.923
Photon energy (eV)	293.2	293.2	293.2

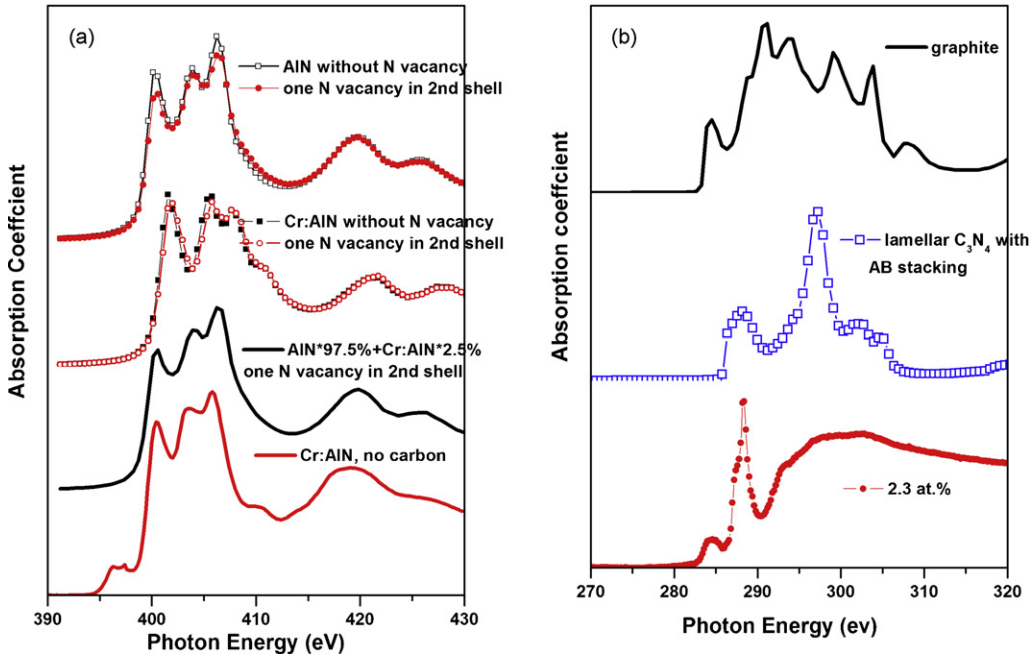

Fig. 6. Simulation of (a) N *K*-edge XANES spectra for AlN and Cr:AlN; (b) C *K*-edge XANES spectra for graphite and lamellar C_3N_4 phase with AB stacking model.

in the first neighboring of N atom, while for AlN, no Cr atom was added. One can see that when N vacancy was considered, the oscillation strengths of peaks B, C and D labeled in Fig. 3 decreased for both AlN and Cr:AlN. The spectrum adding simulation curves of AlN and Cr:AlN together is principally consistent with the experimental result. The missing of pre-edge around 396 eV might be solved by using other first-principal methods. Fig. 6(b) shows the simulations of graphite and lamellar C_3N_4 with AB stacking suggested by Moreau et al. [28]. The characteristic peaks around 284 and 288 eV were presented. However, we did not get totally consistent spectrum with the experimental result when we attempted to add the simulation curves of graphite and lamellar C_3N_4 together. One reason might be that the C–N compounds in our experiments were not totally reacted outcome. Yu et al. have obtained C_3N_4 compounds using ion beam sputtering, similar to our magnetron sputtering [35]. At the same time, they showed that the outcome was not totally reacted. Another reason might be that more precise structure model and calculation methods are needed. When the carbon content increased, defects, disorder and fraction of dopant phases increased also. This induced broadening of the N and C *K*-edge XANES spectra and also brought difficulty for simulation. We therefore concluded the existence of graphite and C–N compounds, in which the fine structures need to be further studied. These dopants would influence the electric and magnetic properties greatly.

3.2. Electric and magnetic properties

Fig. 7 shows the resistivity measured under an alternating current (AC) frequency of 210 Hz and 800 kHz. The resistivity at 210 Hz was higher than $10^5\ \Omega$ cm, while the resistivity at 800 kHz was in the order of $10^3\ \Omega$ cm. The resistivity increased with increasing carbon content under AC frequency of 210 Hz, while it decreased with increasing carbon content under AC frequency of 800 kHz. The resistivity at 800 kHz does not decrease with carbon content monotonically. This error might be due to the contact resistance induced by preparing electrodes. Every sample was measured in high frequency at least 10 times in turn. During the measurement process, the electrodes were stuck firmly and the measured data fluctuated within 8%. Therefore, we believed the error induced by contact was too low to influence resistivity trend. Known from above discussion, the graphite and C–N phases were formed during the deposition process. Normally, the resistivity should decrease with increasing carbon content under a low AC frequency because the graphite is a good conductor. However, the experimental results contradict the conventional speculation. Another feature shown in Fig. 7 was the apparent decrease of resistivity when the AC frequency increased to 800 kHz. These suggest the graphite and C–N phases clusters dispersed in the films. These clusters caused stress to the Cr:AlN crystal lattice because of the lattice mismatch among them. When the current (or voltage) was in some low AC frequency range, the electrons underwent much more scattering at the interface between Cr:AlN and the clusters, which greatly increased the resistivity. When the current (or voltage) was in the high AC frequency range, the mass transfer of carbon, driven by the electric field would occur through the defects, such as the above-mentioned interface. This was

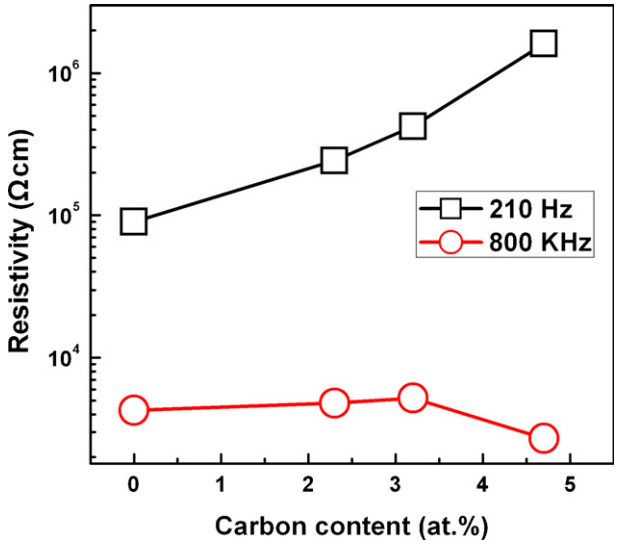

Fig. 7. Variation of resistivity with the C content.

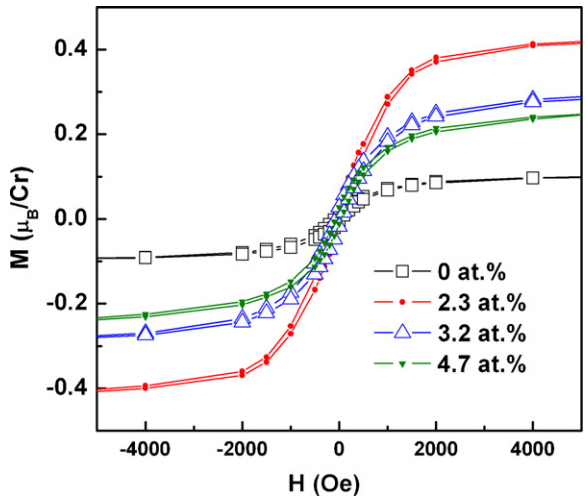

Fig. 8. Variation of AMM with the C content with the carbon content labeled beside every curve.

similar to one of the mechanisms for nonvolatile memory device [3], in which the electrode atoms entered the semiconductor and arrived to the opposite electrode. Also similar effect is electric migration in semiconductor. In these two effects, mass transportation normally occurs along large crystal defects, such as large crystal boundary, and is driven under high power density. For our experiments, the power density in 810 Hz is high, so the carbon mass transfer works well in this high frequency.

Fig. 8 shows the magnetic hystersis loops of all samples. The magnetizations were normalized to the atomic magnetic moment (AMM) of a Cr atom. The apparent hystersis loops proved that the materials were ferromagnetic. The AMM was about 0.1μ_B/Cr for the sample without carbon doping, while for the sample with carbon content of 2.3 at.%, it was about 0.4μ_B/Cr, which might not be the highest because precise carbon content slightly lower or higher than 2.3 at.% was hard to be controlled using sputtering method. The magnetisms of the samples doped by carbon were stronger than that of the sample without carbon doping. Increasing the carbon content did not further increase the AMM. On the contrary, the magnetism weakened for the samples with carbon content of 3.2 and 4.7 at.%. AlN is a semiconductor with wide band gap. Its magnetic mechanism relates to its conductivity after doping [2,36,37]. Since the resistivities of our samples under low AC frequency were about 10^5–10^7 Ω cm, which demonstrated semiconductor–insulator behavior, the bound magnetic polaron (BMP) model was the preferred mechanism of ferromagnetism, in which charged defects trap the electrons surrounding them [2,38]. The trapped electron couples with the magnetic ions within its electron cloud, forming a magnetic ordering entity which is called a BMP. The scope of the BMP is much larger than a single magnetic ion. Thus, a magnetic polaron has more chances of overlapping and interacting with an adjacent BMP to realize magnetic ordering [39,40].

According to BMP theory, the magnetism in semiconductor was expected to be very sensitive to both stress and defects. Normally stress would induce crystal deformation, which weakened the bounded effect for BMPs by crystal field. Defects included dopants, either anion or cation vacancies and interstitials. Experimental and theoretic studies have shown that ferromagnetism can occur or be strengthened when either anion or cation is introduced [41–46]. Normally cation vacancy is difficult to form, but can be stabilized under some special constructions [44]. The usually observed anion vacancy can mediate long-ranged coupling among BMPs [41]. However, too many defects will increase the disorder intensively, which will enhance spin scattering and weaken magnetism. The influences of defect types and amount are reflected in our samples. When the carbon content was small, the introduced stress and N vacancy strengthened strong p–d interaction and long-ranged coupling among local magnetic moments, and then enhanced the AMM quickly. This was shown for the sample with C content of 2.3 at.%. However, increasing carbon content is not favorable for percolation of magnetic moment, because long-ranged correlation of magnetic moments will be interrupted due to too many defect phases Therefore, when carbon content increased further, magnetism weakening was observed for higher carbon content of 3.2 and 4.7 at.%. According to above analysis, there are should be a maximum value of AMM accompanying with variation of C content. However, due to the difficulty in controlling more precise C content in the preparation process, we did not obtained the maximum value and we will try to perform more study to determine variation of magnetism with subtle C doping.

4. Conclusions

Carbon dopant was introduced into the Cr:AlN films. Microstructure analysis demonstrated that when the carbon content was lower than 3.2 at.%, the position of the Cr atom was not significantly affected. The doped carbon atoms formed the graphite phase and the C–N compounds dispersed in the films. The doped carbon influenced the electric and magnetic properties mainly in two aspects. One is that dispersed clusters favored the strengthening of electron scattering so that they enhanced the resistivity under low AC frequency. Atomic migration of carbon might occur under a high AC frequency. Another is that the increased N vacancy and stress brought by the clusters favored coupling among the BMPs and then enhanced the AMM. On the other aspect, too many carbon doping will enhance the disorder and then weaken the magnetic coupling.

Acknowledgements

This work is supported by the Ministry of Science and Technology of China through the National Hi-tech (R&D) project (Nos. 2007AA03Z426 and 2009AA034001) and the National Basic Research Program (No. 2010CB832905), Program for New Century Excellent Talents in University, and the National Natural Science Foundation of China (No. 50772055).

References

[1] A. Mycielski, L. Kowalczyk, R.R. Galazka, R. Sobolewski, D. Wang, A. Burger, M. Sowinska, M. Groza, P. Siffert, A. Szadkowski, B. Witkowska, W. Kaliszek, J. Alloys Compd. 423 (2006) 163.
[2] F. Pan, C. Song, X.J. Liu, Y.C. Yang, F. Zeng, Mater. Sci. Eng. R 62 (2008) 1.
[3] Y.C. Yang, F. Pan, Q. Liu, M. Liu, F. Zeng, Nano Lett. 9 (2009) 1636.
[4] P. Dev, Y. Xue, P.H. Zhang, Phys. Rev. Lett. 100 (2008) 117204.
[5] Z.Q. Yuan, R.R. Du, M.J. Manfra, L.N. Pfeiffer, K.W. West, Appl. Phys. Lett. 94 (2009) 052103.
[6] J.H. Lim, J.H. Shim, J.I. Choi, J.H. Park, W. Kim, J. Joo, C.J. Kim, Physica C 469 (2009) 1182.
[7] H. Kwak, J.R. Chelikowsky, Appl. Phys. Lett. 95 (2009) 263108.
[8] T.S. Herng, S.P. Lau, L. Wang, B.C. Zhao, S.F. Yu, M. Tanemura, A. Akaike, K.S. Teng, Appl. Phys. Lett. 95 (2009) 012505.
[9] S. Khamseh, M. Nose, T. Kawabata, K. Matsuda, S. Ikeno, J. Alloys Compd. 503 (2010) 389.
[10] J.T. Luo, B. Fan, F. Zeng, F. Pan, J. Phys. D: Appl. Phys. 42 (2009) 235406.
[11] A.L. Ankudinov, C.E. Bouldin, J.J. Rehr, J. Sims, H. Hung, Phys. Rev. B 65 (2002) 104107.
[12] B. Ravel, J. Alloys Compd. 401 (2005) 118.
[13] B. Fan, F. Zeng, C. Chen, Y.C. Yang, P.Y. Yang, F. Pan, J. Appl. Phys. 106 (2009) 235406.
[14] F. Zeng, B. Fan, Y.C. Yang, P.Y. Yang, J.T. Luo, C. Chen, F.F. Pan, J. Vac. Sci. Technol. B 28 (2010) 62.
[15] A. Pantelouris, H. Modrow, M. Pantelouris, J. Hormes, D. Reinen, Chem. Phys. 300 (2004) 13.

[16] J.J. Kim, H. Mkino, M. Sakurai, D.C. Oh, T. Hanada, M.W. Cho, T. Yao, S. Emura, S. Kobayashi, J. Vac. Sci. Technol. B 23 (2005) 1308.
[17] T. Takeuchi, Y. Harada, T. Tokushima, M. Taguchi, Y. Takata, A. Chainani, J.J. Kim, H. Makino, T. Yao, T. Yamamoto, T. Tsukamoto, S. Shin, K. Kobayashi, Phys. Rev. B 70 (2004) 245323.
[18] J.A.C. Santana, R. Skomski, V. Singh, V. Palshin, A. Petukhov, Y.B. Losovyj, A. Sokolov, P.A. Dowben, I. Ketsman, J. Appl. Phys. 105 (2009) 07A930.
[19] J.A.C. Santana, V. Singh, V. Palshin, E.M. Handberg, A.G. Petukhov, Y.B. Losovyj, A. Sokolov, I. Ketsman, Appl. Phys. A 98 (2010) 811.
[20] M.L. Werner, P.S. Nico, M.A. Marcus, C. Anastasio, Environ. Sci. Technol. 41 (2007) 4919.
[21] G. Abrasonis, M. Berndt, M. Krause, K. Kuepper, F. Munnik, A. Kolitsch, W. Möller, J. Phys. Chem. C 112 (2008) 17161.
[22] D. Chen, D. Xu, J.J. Wang, B. Zhao, Y.F. Zhang, Thin Solid Films 517 (2008) 986.
[23] R. Kaindl, B. Sartory, J. Neidhardt, R. Franz, A. Reiter, P. Polcik, R. Tessadri, C. Mitterer, Anal. Bioanal. Chem. 389 (2007) 1569.
[24] V. Lughi, D.R. Clarke, Appl. Phys. Lett. 89 (2006) 241911.
[25] M. Bernard, A. Deneuville, O. Thomas, P. Gergaud, P. Sandstrom, J. Birch, Thin Solid Films 380 (2000) 252.
[26] S. Kimura, S. Emura, K. Tokuda, Y.K. Zhou, S. Hasegawa, H. Asahi, J. Cryst. Growth 311 (2009) 2046.
[27] M. Hashimotoa, H. Tanakaa, S. Emuraa, M.S. Kima, T. Honmab, N. Umesakib, Y.K. Zhoua, S. Hasegawaa, H. Asahi, J. Cryst. Growth 273 (2004) 149.
[28] P. Moreau, F. Boucher, G. Goglio, D. Foy, V. Mauchamp, G. Ouvrard, Phys. Rev. B 73 (2006) 195111.
[29] J. Diaz, S. Anders, X. Zhou, E.J. Moler, S.A. Kellar, Z. Hussain, Phys. Rev. B 64 (2001) 125204.
[30] O. Wessely, M.I. Katsnelson, O. Eriksson, Phys. Rev. Lett. 94 (2005) 167401.
[31] J. Stőhr, NEXAFS Spectroscopy, Springer, New York, 1992.
[32] G. Abrasonis, R. Gago, M. Vinnichenko, U. Kreissig, A. Kolitsch, W. Möller, Phys. Rev. B 73 (2006) 125427.
[33] W.S. Chen, J.Q. Zhu, J.C. Han, G. Tian, M.L. Tan, Spectrosc. Spect. Anal. 29 (2009) 268.
[34] M. Jaouen, G. Tourillon, J. Delafond, N. Junqua, G. Hug, Diam. Relat. Mater. 4 (1995) 200.
[35] D.L. Yu, F.R. Xiao, T.S. Wang, Y.J. Tian, J.L. He, D.C. Li, W.K. Wang, J. Mater. Sci. Lett. 19 (2000) 553.
[36] Z.L. Lu, W. Miao, W.Q. Zou, M.X. Xu, M. Zhang, J. Alloys Compd. 494 (2010) 392.
[37] X.J. Liu, X.Y. Zhu, J.T. Luo, F. Zeng, F. Pan, J. Alloys Compd. 482 (2009) 224.
[38] A.J. Behan, A. Mokhtari, H.J. Blythe, D. Score, X.H. Xu, J.R. Neal, A.M. Fox, G.A. Gehring, Phys. Rev. Lett. 100 (2008) 047206.
[39] A. Kaminsk, D.D. Sarma, Phys. Rev. Lett. 88 (2002) 247202.
[40] C. Song, F. Zeng, K.W. Geng, X.J. Liu, F. Pan, B. He, W.S. Yan, Phys. Rev. B 76 (2007) 245215.
[41] W.S. Yan, Z.H. Sun, Z.Y. Pan, Q.H. Liu, T. Yao, Z.Y. Wu, C. Song, F. Zeng, Y.N. Xie, T.D. Hu, S.Q. Wei, Appl. Phys. Lett. 94 (2009) 042508.
[42] H.S. Hsu, J.C.A. Huang, Y.H. Huang, Y.F. Liao, M.Z. Lin, C.H. Lee, J.F. Lee, S.F. Chen, L.Y. Lai, C.P. Liu, Appl. Phys. Lett. 88 (2006) 242507.
[43] W.S. Yan, Z.H. Sun, Q.H. Liu, Z.R. Li, Z.Y. Pan, J. Wang, S.Q. Wei, D. Wang, Y.G. Zhou, X.Y. Zhang, Appl. Phys. Lett. 91 (2007) 062113.
[44] J.B. Yi, C.C. Lim, G.Z. Xing, H.M. Fan, L.H. Van, S.L. Huang, K.S. Yang, X.L. Huang, X.B. Qin, B.Y. Wang, T. Wu, L. Wang, H.T. Zhang, X.Y. Gao, T. Liu, A.T.S. Wee, Y.P. Feng, J. Ding, Phys. Rev. Lett. 104 (2010) 137201.
[45] R.K. Singhal, A. Samariya, Y.T. Xing, S. Kumar, S.N. Dolia, U.P. Deshpande, T. Shripathi, E.B. Saitovitch, J. Alloys Compd. 496 (2010) 324.
[46] Z.L. Lu, X.F. Bian, W.Q. Zou, M.X. Xu, F.M. Zhang, J. Alloys Compd. 492 (2010) 31.